

## $\beta$ Decay Spectra Measurements for the Study of Reactors' Antineutrino Spectra.

G. A. Alcalá<sup>1,\*</sup>, A. Algora<sup>1,2</sup>, M. Fallot<sup>3</sup>, M. Estienne<sup>3</sup>, V. Guadilla<sup>3,\*\*</sup>, W. Galletly<sup>4</sup>, A. Beloeuvre<sup>3</sup>, J.-S. Stutzmann<sup>3</sup>, S. Bouvier<sup>3</sup>, T. Eronen<sup>5</sup>, J. Agramunt<sup>1</sup>, E. Bonnet<sup>3</sup>, D. Etasse<sup>6</sup>, L. Giot<sup>3</sup>, A. Laureau<sup>3</sup>, A. Porta<sup>3</sup>, J. A. Victoria<sup>1</sup>, Y. Molla<sup>3</sup>, J. L. Taín<sup>1</sup>, and the IGISOL collaboration<sup>5</sup>

<sup>1</sup>Instituto de Física Corpuscular (IFIC), València, Spain.

<sup>2</sup>Institute for Nuclear Research (Atomki), Debrecen, Hungary.

<sup>3</sup>SUBATECH, CNRS/IN2P3, IMT Atlantique, Nantes Université, Nantes, France.

<sup>4</sup>Faculty of Physics, University of Warsaw, Warsaw, Poland.

<sup>5</sup>Department of Physics, University of Surrey, Guildford, United Kingdom.

<sup>6</sup>Department of Physics, University of Jyväskylä, Jyväskylä, Finland.

<sup>7</sup>LPC Caen, CNRS/IN2P3, Caen, France.

**Abstract.** Updated reactor antineutrino spectra predictions, based on the Huber-Muller Conversion model, revealed discrepancies known as the Reactor Antineutrino Anomaly (RAA) and the spectral “bump”, raising concerns about the accuracy of the models and data used for these predictions. Consequently, improved nuclear data measurements are essential. The Summation method, an alternative to the Conversion model, may offer more accurate reactor antineutrino spectra predictions. Since a relative small number of fission products significantly contribute to antineutrino spectra in a region where the “bump” is prominent, precise measurements of  $\beta^-$  spectra are crucial. This report presents preliminary steps needed for the analysis of the  $^{92}\text{Rb}$   $\beta^-$  spectrum measured at IGISOL, such as the Monte Carlo model validation.

### 1 Introduction

Nuclear reactor facilities are intense sources of electron antineutrinos ( $\bar{\nu}_e$ ) due to the  $\beta^-$  decays of neutron-rich fission products. These facilities have been widely utilized to study  $\nu$  properties, such as the  $\theta_{13}$  mixing angle [1–3]. The detection of  $\bar{\nu}_e$ s is performed in large scintillator detectors via the inverse beta decay reaction.

Measurements at near baselines (less than 100 m) have revealed discrepancies between the measured and predicted  $\bar{\nu}_e$  spectra, commonly referred to as the Reactor Antineutrino Anomaly (RAA) and the spectral “bump” [1–3]. The RAA is the deficit of measured reactor  $\bar{\nu}_e$ s (flux) relative to theoretical predictions. The “bump” is a distortion in the measured  $\bar{\nu}_e$  energy spectrum, around the 6 MeV kinetic energy region of  $\bar{\nu}_e$ , compared to predictions after renormalization.

There can be several potential sources of these discrepancies. The anomaly could hypothetically arise from unknown physical effects beyond the Standard Model, such as the existence of sterile neutrinos, which might cause the disappearance of  $\bar{\nu}_e$ s at near baselines due to  $\nu$  oscillations. The detection of  $\bar{\nu}_e$ s may be affected by systematic errors associated with the detectors or the methods used for data

gathering. Additionally, there may be inaccuracies in the characterization of fuel of reactors.

To address the questions related to the RAA and the “bump,” the e-shape collaboration aims to improve relevant nuclear data and use more accurate nuclear models employed in the calculation of reactor  $\bar{\nu}_e$  spectra. This is accomplished by precisely measuring the  $\beta^-$  decay spectra of relevant fission fragments associated with the discrepancies found in reactor  $\bar{\nu}_e$  observations. These measurements are essential to determine appropriate models of  $\beta$  feedings and shapes for improving reactor  $\bar{\nu}_e$  spectra predictions.

The conversion method [4, 5] has conventionally been used for calculating reactor  $\bar{\nu}_e$  spectra. It uses the cumulative  $\beta^-$  spectra of the fissile isotopes ( $^{235}\text{U}$ ,  $^{238}\text{U}$ ,  $^{239}\text{Pu}$ , and  $^{241}\text{Pu}$ ) in the fuel of reactors to construct their respective  $\bar{\nu}_e$  spectra by fitting virtual  $\beta^-$  branches to these cumulative  $\beta$  spectra. Recently, Huber and Muller revisited the conversion method [6, 7] by using updated nuclear databases and improving the procedure for calculating  $\bar{\nu}_e$  spectra. Nonetheless, these revisions lead to the RAA and the “bump” [1].

The e-shape collaboration uses the summation method [8, 9] as an alternative to the conversion method. This is an *ab initio* method for calculating  $\bar{\nu}_e$  spectra predictions, where the cumulative  $\beta^-$  ( $\bar{\nu}_e$ ) spectra of reactors are reconstructed from the weighted sum of all of the contributing individual  $\beta^-$  ( $\bar{\nu}_e$ ) spectra of the radioactive isotopes pro-

\*e-mail: galcala@ific.uv.es

\*\*Current address: Faculty of Physics, University of Warsaw, 02-093 Warsaw, Poland

duced in reactors. The total spectrum  $S_k$  of the  $k^{\text{th}}$  fissile isotope is constructed as

$$S_k = \sum_{i,b} A_{k,i} f_{i,b} S_{i,b}, \quad (1)$$

where  $A_{k,i}$  is the activity of the  $i^{\text{th}}$  radioactive isotope,  $f_{i,b}$  is the  $\beta$  feeding of the  $\beta$  transition from the  $i^{\text{th}}$  parent isotope to the  $b^{\text{th}}$  nuclear energy level of the respective daughter isotope, and  $S_{i,b}$  is the  $\beta^-$  ( $\bar{\nu}_e$ ) spectrum of the corresponding  $\beta$  transition. The activity ( $A_{k,i}$ ) of the radioactive isotopes is related to the fission yields of the fission fragments, provided in evaluated databases [10]. Different  $\beta$  feedings ( $f_{i,b}$ ) and  $\beta^-$  ( $\bar{\nu}_e$ ) spectra shape ( $S_{i,b}$ ) models must be compared with accurate experimental data to produce reliable results with the summation method.

$\beta$  feedings can be determined from the de-excitation schemes of daughter nuclei by measuring their  $\gamma$ -rays with HPGe detectors in high-resolution experiments. However, these  $\beta$  feedings may be affected by the Pandemonium effect [11, 12], defined as the overestimation of  $\beta$  feedings to low nuclear energy levels of the daughter nuclei, caused by the low detection efficiency of HPGe detectors for low-intensity and high-energy  $\gamma$ -rays. The Total Absorption Gamma Spectroscopy (TAGS) technique provides experimental  $\beta$  feedings free from the Pandemonium by measuring  $\gamma$ -rays from the de-excitation of daughter isotopes using detectors with high efficiencies that cover almost the whole solid angle around the decaying nuclei [12].

Recent works have put the RAA into question by reducing the flux discrepancy from 6 to 1.9% by employing the summation method with Pandemonium free  $\beta$  feedings [9], utilizing the most reliable experimental data to date [3]. Additionally, it has been proposed that including appropriate nuclear shape factors for first-forbidden  $\beta$  transitions associated with relevant  $\beta^-$  decays that contribute to reactor  $\bar{\nu}_e$  spectra may help to address the issue of the RAA and “bump” [13, 14].

Consequently, accurate  $\beta^-$  spectra measurements to calculate reliable reactor  $\bar{\nu}_e$  spectra predictions are crucial. Among the hundreds of  $\beta^-$  decays that occur in a reactor’s core, around 30 out of 280  $\beta$  decaying levels contribute up to 90% to the total  $\bar{\nu}_e$  spectrum in the energy region where the “bump” is present [15]. Therefore, it is only necessary to measure the most intense  $\beta^-$  decays in this energy region to try to reduce the “bump” [14].

## 2 e-shape detectors

The e-shape collaboration developed two e-shape detectors to measure the shapes of  $\beta^-$  spectra of interest to address the issues in reactor  $\bar{\nu}_e$  spectra observations. These are electron telescopes ( $\Delta E$ - $E$ ) detectors designed to detect electrons in coincidence while rejecting  $\gamma$ -rays [16]. The detector’s  $\Delta E$  part is a thin Si layer of 527  $\mu\text{m}$  thick and an active area of 50×50 mm<sup>2</sup>. The  $E$  part is a plastic scintillator shaped like a truncated pyramid, with its base rounded and its top cut to match the active area of the Si detector. The e-shape detectors reject  $\gamma$ -rays in coincidence because the Si has a negligible efficiency for  $\gamma$ -ray

detection due to its small thickness. Fig. 1 shows an e-shape detector mounted.

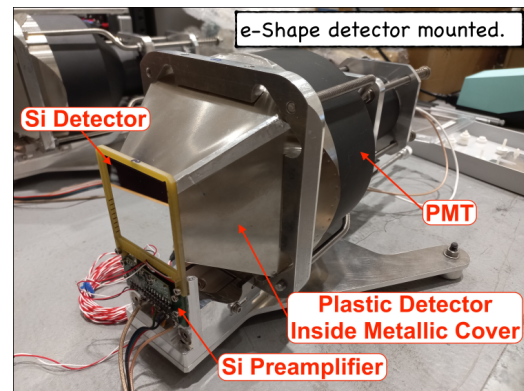


**Figure 1.** e-shape electron telescope detector mounted.

## 3 I233 Experiment

To measure accurate shapes of  $\beta^-$  spectra, it is essential to count with isotopically pure radioactive beams of the isotopes of interest to minimize shape deformations caused by contaminations. The IGISOL-4 facility [17] at the University of Jyväskylä has an online mass separation system capable of generating highly pure radioactive beams suitable for the collaboration. The purification process at IGISOL-4 is performed initially with a dipole magnet, followed by final purification in JYFLTRAP, a state-of-the-art double Penning trap [18].

The e-shape collaboration conducted the I233 experiment at IGISOL-4 in January 2022. Several cases of calibration, Monte Carlo validation, and interest, like the <sup>92</sup>Rb  $\beta^-$  decay, were measured. Radioactive beams were implanted in a tape in front of the e-shape detector within a vacuum chamber. The tape could be periodically moved to reduce the contamination of unstable daughter isotopes on the  $\beta^-$  spectra of the parents.

## 4 Shape Correction Factors

To analyze the experimental data, first it is necessary to validate the Monte Carlo model of the experiment to generate the response matrices of the e-shape detectors. The response matrix is used to perform the deconvolution of the experimental  $\beta^-$  spectra as they are deformed due to the energy distribution of electrons in the plastic detector. To validate the Monte Carlo, simulated spectra must reproduce the corresponding experimental results. To do so, the implemented geometry must accurately reproduce the experimental setup and the models of the shapes of simulated spectra have to account for the physical phenomena that affect the shapes of the measured  $\beta^-$  spectra.

The shape of the  $\beta$  decay spectrum, accounting for the Fermi theory of  $\beta$  decay and including nuclear and atomic effects, can be written in natural units as

$$S(W) \propto \eta W(W_0 - W)^2 F_0(Z, W) C(Z, W) K(Z, W), \quad (2)$$

where  $\eta W(W_0 - W)^2$  is known as the statistical factor, with  $\eta$  representing the electron momentum,  $W$  the total electron energy, and  $W_0$  the maximum total electron energy for the corresponding  $\beta^-$  transition.  $F_0(Z, W)$  is the Coulomb Fermi function, where  $Z$  is the atomic number of the daughter isotope.  $C(Z, W)$  is the nuclear shape factor, which accounts for the nuclear structure information, and  $K(Z, W)$  contains other higher-order correction factors that consider additional atomic, nuclear, and weak interaction effects [19].

For allowed transitions, nuclear shape factors can be considered as 1, as they do not depend on the electron kinetic energy. Conversely, nuclear shape factors for forbidden transitions vary with the electron kinetic energy, making them case-dependent and requiring the calculation of specific form factors [14]. In the I233 experiment, both allowed and first-forbidden  $\beta^-$  spectra were measured. Nuclear shape factor corrections for relevant first-forbidden  $\beta^-$  transitions, calculated by [14], can be used to generate simulated and predicted spectra for the corresponding measured cases. Additionally, sets of allowed shape correction factors proposed by Huber [6] and Hayen et al. [19] can be included in  $K(Z, W)$ .

The allowed shape correction factors used in this work were the finite size of the nucleus, weak interaction finite size of the nucleus, radiative correction, atomic screening, atomic exchange, atomic mismatch, nuclear recoil, distorted Coulomb potential due to recoil, and weak magnetism terms [6, 19].

## 5 Monte Carlo Validation

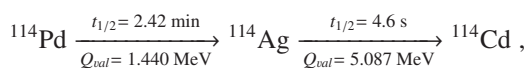
The analysis of the experimental data relies on the deconvolution of the measured  $\beta^-$  spectra. This procedure is essential as measured coincidence spectra are distorted due to the incomplete absorption of the energy of electrons in the plastic detector. The original  $\beta^-$  spectrum is obtained by solving the inverse problem

$$\vec{d} = \mathcal{R} \cdot \vec{\delta} + \vec{C} \quad (3)$$

using iterative deconvolution algorithms [20], where  $\vec{d}$  is the experimental  $\beta^-$  spectrum,  $\mathcal{R}$  is the response matrix of an e-shape detector,  $\vec{\delta}$  is the original (deconvoluted) spectrum, and  $\vec{C}$  represents the contributions from background and contaminants.

The response matrix for each e-shape detector is constructed using simulated spectra of monoenergetic electrons. For this purpose, Geant4 simulations [21] are employed. As noted above, to reproduce the experimental results with the corresponding simulated spectra, the Monte Carlo model must accurately replicate the experimental setup and account for the physical interactions of the particles. If the simulations successfully reproduce the experimental data, the Monte Carlo model is considered validated, allowing for the calculation of reliable response matrices.

The  $^{114}\text{Pd}$ - $^{114}\text{Ag}$   $\beta^-$  decay chain, given by the scheme



was measured for validation and calibration purposes. This decay chain was selected as their decays are dominated by allowed transitions, with  $\beta^-$  feedings well-determined from high-resolution experiments, as reported in the ENSDF database [22–24]. Fig. 2 shows the measured  $^{114}\text{Pd}$ - $^{114}\text{Ag}$   $\beta^-$  spectrum compared with simulated spectra generated with ENSDF  $\beta^-$  feedings and shape models based on the Fermi Function alone, Hayen corrections [19] with the Weak Magnetism term, and Huber corrections [6].

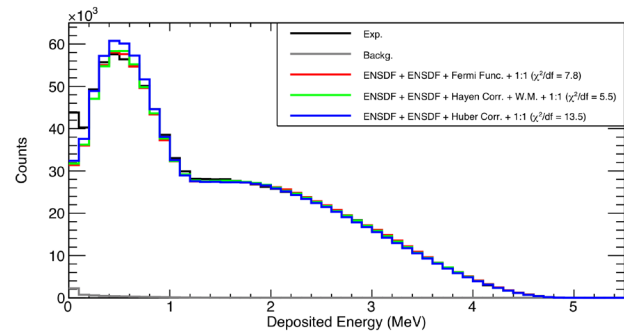


**Figure 2.** Comparisons of the  $^{114}\text{Pd}$ - $^{114}\text{Ag}$  experimental  $\beta^-$  spectrum against simulated spectra for the validation of the Monte Carlo model.

Fig. 2 shows that the simulated spectra suitably reproduce the experimental data. Fig. 3 illustrates the corresponding relative differences between the simulated and experimental spectra. The relative differences are around 3% in most of the energy regions of the parent and daughter nuclei decays. These values confirm the successful validation of the Monte Carlo model, as they fulfill the established criterion for this study, which requires relative differences below 5% for validation.

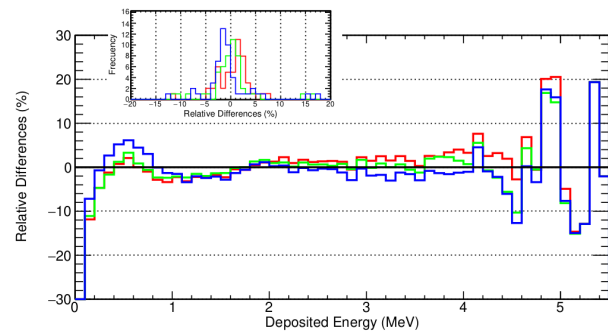


**Figure 3.** Relative differences of the simulated spectra respect to the  $^{114}\text{Pd}$ - $^{114}\text{Ag}$  experimental  $\beta^-$  spectrum.

## 6 Spectra Analysis

After validating the Monte Carlo model, response matrices for the e-shape detectors were constructed using simulated spectra of monoenergetic electrons with kinetic energies ranging from 20 to 9000 keV, in steps of 20 keV. Fig. 4 presents a 3-D view of the calculated response matrix



for one of the e-shape detectors. The x-axis, referred to as “DATA channels”, represents the channels of the simulated spectra, which correspond to the deposited energies of the electrons in the plastic detector. The y-axis, labeled as “MODEL channels”, represents the initial kinetic energies of the simulated electrons, which correspond to the expected energies of the detected electrons.

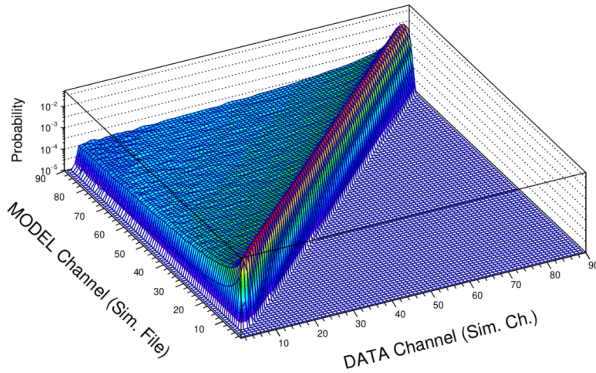


**Figure 4.** 3-D view of the normalized response matrix for performing deconvolutions to the plastic coincidence  $\beta^-$  spectra.

The calculated response matrix must then be included in Eq. (3), to solve the equation iteratively to obtain the original (deconvoluted) spectra using the Expectation-Maximization deconvolution method based on the Bayes theorem [20]. The  $^{92}\text{Rb}$  experimental  $\beta^-$  spectrum, presented in Fig. 5, is expected to be deconvoluted using the tools mentioned in this report.

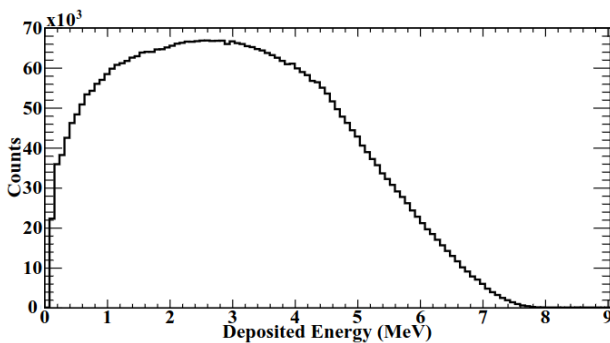


**Figure 5.** Measured  $^{92}\text{Rb}$  coincidence  $\beta$  spectrum registered in the plastic detector [25].

As commented above, to obtain reliable deconvolutions, it is important to consider that the daughter nucleus of  $^{92}\text{Rb}$ ,  $^{92}\text{Sr}$ , is unstable and has a half-life comparable to that of the parent nucleus. Consequently, tape moving cycles were required for the  $^{92}\text{Rb}$  decay measurements to reduce the contamination from the  $\beta^-$  decays of the daughter on the parent spectrum. For the case of the  $^{92}\text{Rb}$ , the tape was moved every 22.49 s. Theoretical and experimental values for the contamination proportion of  $^{92}\text{Sr}$  were determined and used to clean the  $^{92}\text{Rb}$  experimental  $\beta^-$  spectrum, using simulations of the contaminating spectra.

## 7 Conclusion

This report shows improvements in the validation process of the Monte Carlo model of the I233 experiment compared with previous results reported in the NSD2022 conference [25]. This achievement is related to a better determination of the calibration of the experimental data. Future works will show the results of the ongoing deconvolution of the  $^{92}\text{Rb}$  experimental  $\beta$  spectrum, among other cases of relevancy for explaining the RAA and “bump”.

We acknowledge the help and support of the IGISOL group in the measurements. This work has been supported by the Ministry of Science and Innovation of Spain grant No. PID2019-104714GB-C21, the Generalitat Valenciana Santiago Grisolfá program grants, Generalitat Valenciana under Prometeo Grant CIPROM/2022/9, the SANDA project funded under H2020-Euratom-1.1. grant No. 847552, the CNRS challenge NEEDS and the associated NACRE project, as well as the CHANDA FP7/EURATOM project (Contract No. 605203), and the CNRS/in2p3 Master projects Jyväskylä and OPALE. We also acknowledge the financial support from the Ministerio de Ciencia e Innovación with funding from the European Union NextGenerationEU and Generalitat Valenciana in the call Programa de Planes Complementarios de I+D+i (PRTR 2022) under Project DETCOM, reference ASFAE/2022/027 and Ministerio de Ciencia e Innovación PID2022-138297NB-C21.

## References

- [1] G. Mention *et al.*, Phys. Rev. D **83**, 073006 (2011).
- [2] J. H. Choi *et al.*, Phys. Rev. Lett. **116**, 211801 (2016).
- [3] F. P. An *et al.*, Chin. Phys. C **41**, 013002 (2017).
- [4] Schreckenbach *et al.*, Phys. Lett. B **99**, 251 (1981).
- [5] Schreckenbach *et al.*, Phys. Lett. B **160**, 325 (1985).
- [6] P. Huber, Phys. Rev. C **84**, 24617 (2011).
- [7] Th. A. Muller *et al.*, Phys. Rev. C **83**, 054615 (2011).
- [8] King & Perkins, Phys. Rev. **112**, 963 (1958).
- [9] M. Estienne *et al.*, Phys. Rev. Lett. **123**, 022502 (2019).
- [10] A. J. M. Plompen *et al.*, Eur. Phys. J. A **56**, 181 (2020).
- [11] J. C. Hardy *et al.*, Phys. Lett. B **71-2**, 307 (1977).
- [12] A. Algora *et al.*, Eur. Phys. J. A **57**, 85 (2021).
- [13] A. C. Hayes, *et al.*, Phys. Rev. Lett. **112**, 202501 (2014).
- [14] L. Hayen *et al.*, Phys. Rev. C **100**, 054323 (2019).
- [15] A. A. Sonzogni *et al.*, Phys. Rev. Lett. **119**, 112501 (2017).
- [16] V. Guadilla *et al.*, JINST **19**, P02027 (2024).
- [17] I. D. Moore *et al.*, Hyperfine Interact. **223**, 17 (2014).
- [18] T. Eronen *et al.*, Eur. Phys. J. A **48**, 46 (2012).
- [19] L. Hayen *et al.*, Rev. Mod. Phys. **90**, 015008 (2018).
- [20] J. L. Tain & D. Cano-Ott, Nucl. Instrum. Methods. Phys. Res. A **571** 728 (2007).
- [21] J. Allison *et al.*, Methods Phys. Res. A **835**, 186 (2016).
- [22] V. Koponen *et al.*, Z. Physik A **333**, 339 (1989).

- [23] J. Rogowski *et al.*, Univ. Mainz, 1985 Ann. Rept., 8 (1986).  
[24] E. Lund & B. Fogelberg, Z Physik A **315**, 295 (1984).

- [25] G. A. Alcalá *et al.*, EPJ Web of Conf. **284**, 08001 (2023).